

Article

# Comprehensive Experimental Study on the Thermophysical Characteristics of DI Water Based $\text{Co}_{0.5}\text{Zn}_{0.5}\text{Fe}_2\text{O}_4$ Nanofluid for Solar Thermal Harvesting

Tsogtbilegt Boldoo, Jeonggyun Ham and Honghyun Cho \* 

Department of Mechanical Engineering, Chosun University, Gwangju 61452, Korea; tsogtbilegt31@gmail.com (T.B.); orchiders@chosun.kr (J.H.)

\* Correspondence: hhcho@chosun.ac.kr; Tel.: +82-62-230-7050; Fax: +82-62-230-7055

Received: 10 November 2020; Accepted: 24 November 2020; Published: 26 November 2020



**Abstract:** The thermophysical properties of water-based  $\text{Co}_{0.5}\text{Zn}_{0.5}\text{Fe}_2\text{O}_4$  magnetic nanofluid were investigated experimentally. Consequently, the viscosities of 0.25 wt% and 1 wt%  $\text{Co}_{0.5}\text{Zn}_{0.5}\text{Fe}_2\text{O}_4$  nanofluid were 1.03 mPa·s and 1.13 mPa·s, each greater than that of the 20 °C base fluid (water), which were increased by 7.3% and 17.7%, respectively. The  $\text{Co}_{0.5}\text{Zn}_{0.5}\text{Fe}_2\text{O}_4$  nanofluid thermal conductivity enhanced from 0.605 and 0.618 to 0.654 and 0.693 W/m·°C at concentrations of 0.25 wt% and 1 wt%, respectively, when the temperature increased from 20 to 50 °C. The maximum thermal conductivity of the  $\text{Co}_{0.5}\text{Zn}_{0.5}\text{Fe}_2\text{O}_4$  nanofluid was 0.693 W/m·°C at a concentration of 1 wt% and a temperature of 50 °C. Furthermore, following a solar exposure of 120 min, the photothermal energy conversion efficiency of 0.25 wt%, 0.5 wt%, 0.75 wt%, and 1 wt%  $\text{Co}_{0.5}\text{Zn}_{0.5}\text{Fe}_2\text{O}_4$  nanofluids increased by 4.8%, 5.6%, 7.1%, and 4.1%, respectively, more than that of water.

**Keywords:**  $\text{Co}_{0.5}\text{Zn}_{0.5}\text{Fe}_2\text{O}_4$  nanofluid; cobalt-zinc ferrite; thermal conductivity; PTEC (photothermal energy conversion) efficiency; optical absorption; viscosity

## 1. Introduction

Thermal energy has taken an exceptional role in human transformation of the environment since the dawn of time. Due to rapid technological development, annual average electrical energy per capita consumption increased drastically to as much as 3132.5 kWh in 2014, creating a global energy crisis [1]. There has been an unprecedented burning of conventional fossil fuels to meet this enormous energy demand in developed countries [1]. However, to meet this demand in an environmentally sustainable manner, the world must surmount multiple challenges, e.g., discovering affordable and sustainable alternative green energy sources. Among various energy sources, solar energy shows the most potential as a solution to this pressing problem. However, while the technology for obtaining heat from solar energy has been in use for a long time, the scope of its application and systems has been very limited because of low energy conversion efficiency and low energy density.

In many thermal energy systems, heat transfer efficiency is the most important factor in increasing system efficiency. Methods to enhance the heat transfer are divided into two classifications: active and passive enhancement methods [2]. In active heat transfer enhancement, the system requires additional external energy input, e.g., through mechanical stirring, vibration, circulation, and external magnetic or external fields. However, these approaches are usually expensive and are inapplicable under certain operating conditions. In passive heat transfer enhancement, heat transfer improvement is accomplished by altering properties of the working fluids, changing surface area available for heat

transfer exchanger [3–6]. Among passive heat transfer enhancement approaches, using nanomaterials to improve properties of the thermal system has been attracting researches recently [7–12].

Nanofluids, as described by Choi et al., are working fluids containing functionalized nanomaterials smaller than 100 nm [13]. Depending on the desired application, characteristics of the nanofluid can be altered by changing size, shape, or concentration of the nanomaterial. A major beneficial application of nanofluids is its use in thermal systems, especially the solar thermal collector system for which nanofluids are working fluids with enhanced optical and thermal characteristics. Furthermore, using nanofluids can increase photothermal conversion energy efficiency [14–22] in a solar thermal harvesting systems. Some nanoparticles exhibit different behavior by magnetic effect and are called magnetic particles or ferrofluid nanoparticles. These so-called magnetic nanoparticles are usually metal oxides such as  $\gamma$ -Fe<sub>2</sub>O<sub>3</sub>, Fe<sub>3</sub>O<sub>4</sub>, Co<sub>3</sub>O<sub>4</sub>, and spinel-type composites such as MFe<sub>2</sub>O<sub>4</sub> (M = Mn, Co, Zn, or Ni) [23].

Various synthesis techniques have been utilized to manufacture ferrite nanoparticles with characteristics different from the bulk material characteristics. Of these synthesis techniques, including sol–gel, chemical coprecipitation, and hydrothermal techniques, the chemical coprecipitation method is predominantly used because of its simplicity and economics. According to Novopashin et al. [24], the first manufacturing method for magnetic nanoparticles, in 1965, was to grind bulk Fe<sub>3</sub>O<sub>4</sub> materials in a ball mill [25]. However, there are several disadvantages to this method, including contamination, low productivity, and inability to control particle size. Moreover, oleic acid and heptane are used to achieve good dispersion stability in the Fe<sub>3</sub>O<sub>4</sub> nanofluid. Hence, a chemical coprecipitation technique known as the chemical codeposition method has been adopted in this research field. Typically, this method employs the precipitation of Fe<sup>2+</sup> and Fe<sup>3+</sup> salts in a water medium with an alkali such as NaOH and KOH added at a low temperature. Intense stirring methods are applied to the solution to control nanoparticle size. This synthesis method facilitates the manufacture of controlled sized magnetic nanoparticles at comparably high efficiency and low temperature. In a study by Lopez et al. [26], Co<sub>(1-x)</sub>Zn<sub>x</sub>Fe<sub>2</sub>O<sub>4</sub> nanoparticles were deposited using cobalt (II) chloride hexahydrate, iron (III) chloride hexahydrate, and zinc sulfate heptahydrate in NaOH water solution at 80 °C. These nanoparticles exhibited fine ferrite nanoparticle behavior in vibrating sample magnetometry and X-ray diffraction (XRD) and vibrating sample magnetometry (VSM) tests. Table 1 presents a summary of the magnetic nanofluid preparation [27–38]. Currently, a water-based Fe<sub>3</sub>O<sub>4</sub> nanofluid is widely used, but there has been hardly any research into alternatives. Moreover, the two-step nanofluid manufacturing technique is broadly applied in the industrial field because of its simplicity and reliability. In Table 1, most of the nanofluids are composed of nanoparticles smaller than 20 nm because the nanofluid’s thermal conductivity has a tendency to increase as the nanoparticles size decreases [39].

**Table 1.** Summary of magnetic nanofluid preparation.

Reference	Particles	Diameter (nm)	Base Fluid	Concentration
[27]	Fe <sub>3</sub> O <sub>4</sub>	6.7	Kerosene	0–7.8 vol%
[28]	$\alpha$ -Fe <sub>2</sub> O <sub>3</sub>	5	Glycerol	0.155–0.75 vol%
[29]	$\gamma$ -Fe <sub>2</sub> O <sub>3</sub>	8–15	H <sub>2</sub> O, n-decane	65–300 g/L
[30]	Fe <sub>3</sub> O <sub>4</sub> , CoFe <sub>2</sub> O <sub>4</sub>	1e	H <sub>2</sub> O	2–6.5 vol%
[31]	Fe <sub>3</sub> O <sub>4</sub>	10	H <sub>2</sub> O	0–4.8 vol%
[32]	ND, Ni	30	H <sub>2</sub> O/EG	0–3.03 wt%
[33]	Fe <sub>3</sub> O <sub>4</sub>	10	H <sub>2</sub> O, kerosene	1–7 wt%
[34]	Fe <sub>3</sub> O <sub>4</sub> , Fe	60, 35–45	H <sub>2</sub> O	0.86 vol%
[35]	Fe <sub>3</sub> O <sub>4</sub> , Mn-Zn	6.7	Kerosene	0–10 vol%
[36]	Ni Fe <sub>2</sub> O <sub>3</sub>	50	Kerosene	5, 10 vol%
[37]	CoFe <sub>2</sub> O <sub>4</sub>	14	H <sub>2</sub> O	0.2–1 vol%
[38]	Fe <sub>3</sub> O <sub>4</sub>	11	H <sub>2</sub> O	0.2–1 vol%

Li et al. [40] reported a remarkable dependence of  $\text{Fe}_3\text{O}_4$  magnetic nanofluid properties on the magnetic field strength and its direction. They result posits that a direction of the magnetic field aligned with the temperature distribution of nanofluid has more potential for improving thermal conductivity than when it is perpendicular. The energy transfer efficiency enhanced because nanoparticles in the nanofluid tended to arrange a chainlike formation along the magnetic field direction that aligned with temperature distribution in a nanofluid. Natami et al. [41] investigated a magnetic effect on convective heat transfer of  $\text{Fe}_3\text{O}_4$  nanofluid in a horizontal pipe. They concluded the heat transfer significantly increases in the laminar regime with a high concentration of  $\text{Fe}_3\text{O}_4$  nanofluid. Furthermore, in some cases, heat transfer decreases while Hartmann's number increases. They assumed that this was because the accompanying decrease in Brownian motion was caused by the strong magnetic field. An investigation by Sun et al. [3] examined the magnetic effect on convective heat transfer of  $\text{Fe}_3\text{O}_4$  nanofluid in a pipe. Heat transfer via 0.9 vol%  $\text{Fe}_3\text{O}_4$  nanofluid enhanced convective heat transfer by 9.16% at  $\text{Re} = 1080$  compared with the base fluid. They reported the convective heat transfer enhancement from the  $\text{Fe}_3\text{O}_4$  nanofluid was more notable in a gradient magnetic field than a uniform magnetic field. Based on their results, the flow frictional resistance of  $\text{Fe}_3\text{O}_4$ -water in a thermal system is less significant than the improvement to heat transfer. In a study on surface cooling based thermomagnetic convection, Zablotsky et al. [42] found that the cooling intensity of a ferrofluid improved significantly around the maximal magnetic field intensity with more intense heat transfer.

The finite supply of conventional fuels combined with the issue of climate change has placed humanity on the cusp of restricting the use of fossil fuels. Thus, research on developing systems powered by renewable energy and on improving the system performance of such systems is crucial. Particularly critical studies are on improving heat transfer and heat absorption efficiency of systems that produce heat energy via renewable energy. Against this background, there has been a radical increase in the study of magnetic nanofluids in solar energy harvesting systems within the research community. Furthermore, this flourishing attraction within this field has led to numerous studies and the creation of research literature on magnetic nanofluids such as  $\text{Fe}_3\text{O}_4$ ,  $\text{Fe}_2\text{O}_4$ , and  $\text{ND-Co}_3\text{O}_4$ . However, while the thermal and magnetic properties of various magnetic nanofluids have been extensively investigated, there are still uninvestigated magnetic nanofluids (e.g.,  $\text{Co}_{0.5}\text{Zn}_{0.5}\text{Fe}_2\text{O}_4$  nanofluid) that may have promising properties. The key objective of this work is to experimentally investigate and analyze the thermal properties of diluted water (DI-water) based  $\text{Co}_{0.5}\text{Zn}_{0.5}\text{Fe}_2\text{O}_4$  magnetic nanofluid. To thoroughly characterize the  $\text{Co}_{0.5}\text{Zn}_{0.5}\text{Fe}_2\text{O}_4$  particles, XRD, transmission electron microscopy (TEM) imaging, and VSM tests were conducted. Through this study, we aim to increase the understanding of  $\text{Co}_{0.5}\text{Zn}_{0.5}\text{Fe}_2\text{O}_4$  magnetic nanofluid, which is a new applicable nanofluid, and to investigate its applicability in various systems.

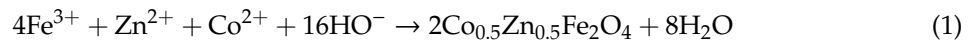
## 2. Nanoparticles and Experimental Methods

### 2.1. $\text{Co}_{0.5}\text{Zn}_{0.5}\text{Fe}_2\text{O}_4$ Nanofluid

Nanofluids are complex colloids that disperse functionalized nanomaterials in broadly used working agents such as refrigerant, thermal oil, antifreeze, and water. In a nanofluid, solid materials within the nanofluid tend to settle to the bottom of the liquid due to the force of gravity. This precipitation of nanomaterials can cause a direct unfavorable influence on the operation of a thermal system such as clogging the pump and polluting the heat transfer surface. Thus, the manufacture of nanofluids with superior dispersal dynamics is a major concern in nanofluid application.

The procedure for manufacturing  $\text{Co}_{0.5}\text{Zn}_{0.5}\text{Fe}_2\text{O}_4$  nanofluid includes synthesis of the  $\text{Co}_{0.5}\text{Zn}_{0.5}\text{Fe}_2\text{O}_4$  nanoparticle and homogenous nanoparticle distribution in the base fluid, which constitutes the two-step manufacturing method extensively used at both the research and industrial level.  $\text{Co}_{0.5}\text{Zn}_{0.5}\text{Fe}_2\text{O}_4$  nanoparticles are prepared via chemical coprecipitation using cobalt chloride ( $\text{CoCl}_2$ ), zinc sulfate ( $\text{ZnSO}_4$ ), and iron (III) chloride ( $\text{FeCl}_3$ ). DI water and oleic acid are used

as the base fluid and coating agent, respectively. The chemical balance equation for  $\text{Co}_{0.5}\text{Zn}_{0.5}\text{Fe}_2\text{O}_4$  is described by Equation (1) [26].



For the chemical coprecipitation method, 8.10 gr of  $\text{FeCl}_3 \cdot 6\text{H}_2\text{O}$ , 1.78 gr of  $\text{CoCl}_2 \cdot 6\text{H}_2\text{O}$ , and 2.15 gr of  $\text{ZnSO}_4 \cdot 7\text{H}_2\text{O}$  were dissolved in 225 mL of DI water and heated until the temperature reached 80 °C. A second mixture was prepared using 56 mL of NaOH (4 mol/L) and 18.75 mL of DI water. The second mixture was added dropwise to the first mixture with magnetic mixing at 80 °C. The precipitated  $\text{Co}_{0.5}\text{Zn}_{0.5}\text{Fe}_2\text{O}_4$  nanoparticles were heated at 80 °C. After heating for 1 h, mixture was maintained at room temperature until its temperature reached 25 °C. After chemical reaction and cooling, the  $\text{Co}_{0.5}\text{Zn}_{0.5}\text{Fe}_2\text{O}_4$  nanoparticle precipitation was separated from the reactants using a magnetic bar and washed in DI water at least three times. Subsequently, pure  $\text{Co}_{0.5}\text{Zn}_{0.5}\text{Fe}_2\text{O}_4$  nanoparticles were coated with the oleic acid surfactant at a pH maintained within 10–11 using NaOH. To disperse the  $\text{Co}_{0.5}\text{Zn}_{0.5}\text{Fe}_2\text{O}_4$  nanoparticles in a DI water base fluid, the nanoparticles and base fluid were dispersed by using ultrasonication at 20 kHz for 2 h. The nanofluid was prepared at concentrations of 0 wt%, 0.25 wt%, 0.5 wt%, 0.75 wt%, and 1 wt%.

Figure 1 presents a picture of  $\text{Co}_{0.5}\text{Zn}_{0.5}\text{Fe}_2\text{O}_4$  nanofluid of varying weight concentrations (0 wt %, 0.25 wt%, 0.5 wt%, 0.75 wt%, and 1 wt%). As illustrated in Figure 1, with an observation test, it can be seen that  $\text{Co}_{0.5}\text{Zn}_{0.5}\text{Fe}_2\text{O}_4$  nanofluid is relatively dark brown compared to the base fluid. The nanofluid samples exhibit good dispersion stability, as sedimentation and separation have not been observed in the suspensions after multiple experiments at various temperatures over the course of two months.

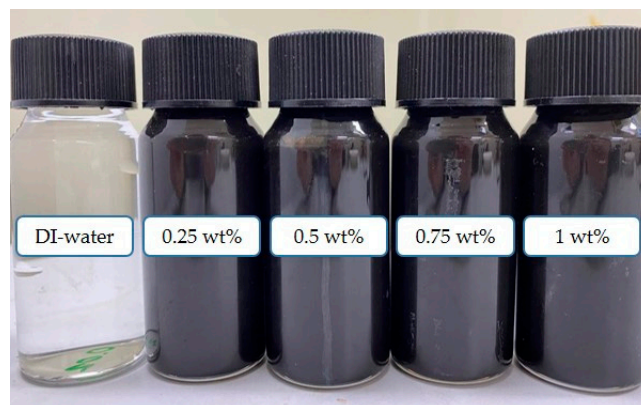


**Figure 1.**  $\text{Co}_{0.5}\text{Zn}_{0.5}\text{Fe}_2\text{O}_4$  nanofluid of varying concentrations.

To conduct the experiment satisfactorily, preliminary test was carried out to decide the optimal concentration of the  $\text{Co}_{0.5}\text{Zn}_{0.5}\text{Fe}_2\text{O}_4$  nanofluid. The  $\text{Co}_{0.5}\text{Zn}_{0.5}\text{Fe}_2\text{O}_4$  nanofluid with a lower concentration than 0.1 wt% exhibited insignificant thermal conductivity and photothermal energy conversion performance, therefore it cannot be acceptable. Moreover,  $\text{Co}_{0.5}\text{Zn}_{0.5}\text{Fe}_2\text{O}_4$  nanofluid with a higher concentration caused serious problems over its merits such as high viscosity and low dispersion stability. For example, too high a concentration of nanofluid is too sensitive to the high temperature, thus it can cause pump and pipe clogging in the thermal system.

The crystal structure of  $\text{Co}_{0.5}\text{Zn}_{0.5}\text{Fe}_2\text{O}_4$  nanoparticles was tested using an X-ray diffractometer on the  $2\theta$  scale using  $\text{CuK}\alpha$  radiation ( $\lambda = 0.15443 \text{ \AA}$ , 16 mA, and 40 kV) at room temperature, with the beam angle ranging from 20 to 100° and a step time of 1 s. The reflection of the diffraction pattern were classified and investigated by an X'Pert<sup>3</sup> MRD XL diffractometer (Malvern Panalytical, Malvern, UK). In order to assess the size of  $\text{Co}_{0.5}\text{Zn}_{0.5}\text{Fe}_2\text{O}_4$  nanoparticles, Scherrer's Equation (2) [43] was used.

$$d = \frac{k\lambda}{\beta \cos \theta} \quad (2)$$

where  $d$  is the diameter of the nanoparticle (nm),  $k = 0.9$  is the Scherrer constant,  $\lambda$  is the wavelength of the X-ray source (0.15406 nm),  $\beta$  is the full width of the powder reflection, and  $\theta$  is the peak position for reflection.

The size and morphology of the synthesized  $\text{Co}_{0.5}\text{Zn}_{0.5}\text{Fe}_2\text{O}_4$  nanoparticles were examined via high-resolution TEM image tests. The TEM tests were conducted using a JEM-2100F (JEOL LTD, Akishima, Japan) analytical electron microscope. Using the TEM results, the distribution and diameter of the  $\text{Co}_{0.5}\text{Zn}_{0.5}\text{Fe}_2\text{O}_4$  nanoparticles in the base fluid (DI water) were analyzed in ImageJ software 1.8.0.

An important point of focus with magnetic nanoparticles is magnetization property that is nanoparticles direction and it can control with a direction of magnetic field. The magnetic properties are categorized based on their reaction in a magnetic field. Magnetization of  $\text{Co}_{0.5}\text{Zn}_{0.5}\text{Fe}_2\text{O}_4$  nanoparticles tested using an 8600 VSM Series (Lake Shore Cryotronics, Westerville, OH, USA) vibrating sample magnetometer. The applied magnetic field ranged from  $-10,000$  to  $10,000$  Gs at room temperature ( $25\text{ }^\circ\text{C}$ ).

A concern for further development and application of nanofluids is the poor nanofluid dispersion stability, which can aggressively impact the rheological and thermophysical properties of working fluid. A Zeta potential analyzer (ELSZ-2000, Otsuka Electronics Co., Ltd., Osaka, Japan), which works on the dynamic light scattering (photon correlation technique) principle, was utilized to examine dispersion stability of the  $\text{Co}_{0.5}\text{Zn}_{0.5}\text{Fe}_2\text{O}_4$  nanofluid. To obtain precise data on stability, the samples were tested at least three times at room temperature ( $25\text{ }^\circ\text{C}$ ). In addition to the zeta potential test, an observation test was conducted on the samples to inspect the dispersion stability of  $\text{Co}_{0.5}\text{Zn}_{0.5}\text{Fe}_2\text{O}_4$  nanofluid.

## 2.2. Experimental Setup

An AvaSpec-ULS2048 spectrometer and an AvaLight light source (Avantes, Apeldoorn, The Netherlands) were utilized to examine the optical characteristics of the  $\text{Co}_{0.5}\text{Zn}_{0.5}\text{Fe}_2\text{O}_4$  nanofluid. Tests were conducted in the UV-Vis spectral wavelength range  $300\text{--}1300$  nm at room temperature ( $25\text{ }^\circ\text{C}$ ). To verify the reliability of the results obtained, each sample was tested in a 10 mm wide quartz cuvette at least three times.

Of the nanofluid characteristics, viscosity is a particularly critical property, which indicates fluid's resistance to flow and directly affects pressure drop and pump power consumption in a heat transfer process. The viscosity of  $\text{Co}_{0.5}\text{Zn}_{0.5}\text{Fe}_2\text{O}_4$  nanofluid was measured using an SV-10 viscometer (A&D, Limited, Tokyo, Japan), which uses the tuning fork measurement method. The operating temperature of the test samples was varied from  $20$  to  $50\text{ }^\circ\text{C}$  to examine the temperature effect on viscosity of  $\text{Co}_{0.5}\text{Zn}_{0.5}\text{Fe}_2\text{O}_4$  nanofluid.

KD2-Pro (Decagon Devices, Inc., Pullman, WA, USA) analyzer was utilized to measure the thermal conductivity of the  $\text{Co}_{0.5}\text{Zn}_{0.5}\text{Fe}_2\text{O}_4$  nanofluid. The KD2-Pro thermal properties analyzer experiments were performed by applying the transient hot-wire technique. As presented in Figure 2, a metal probe was immersed in the test samples, which had full contact with the surrounding test sample. Furthermore, a thermal constant bath was connected to a double jacket beaker to stabilize the inside temperature. The measured data was verified by testing samples at least four times at 20 min intervals. To examine temperature effect on the thermal conductivity of  $\text{Co}_{0.5}\text{Zn}_{0.5}\text{Fe}_2\text{O}_4$  nanofluid, the temperature of nanofluid was varied from  $20$  to  $50\text{ }^\circ\text{C}$ .

Figure 3 presents picture and schematics of the PTEC (photothermal energy conversion) experiment setup. The capacity of the sample beaker was 40 mL, and it was placed directly beneath a halogen lamp functioning as a solar simulator. The incident solar irradiance and ambient temperatures were fixed at  $650\text{ W/m}^2$  and  $20\text{ }^\circ\text{C}$ , respectively. Thermal insulation with  $0.025\text{--}0.04\text{ W/m}\cdot^\circ\text{C}$  was applied to prevent heat loss. To absorb solar energy in the nanofluid, the top of the sample container was made with glass. The temperature gradient of the nanofluid in the sample beaker was examined by using three K-type thermocouples, which was placed at the top, middle, and bottom of the sample container. PTEC efficiency is a measure of how much solar energy is converted to the heat in the sample fluid. The PTEC efficiency can be expressed as Equation (3) [44]

$$\eta = \frac{c_{nf}m_{nf}\Delta\bar{T}}{IA\Delta t} \tag{3}$$

where  $m_{nf}$  and  $c_{nf}$  are the nanofluid mass and specific heat,  $\Delta\bar{T}$  is nanofluid average temperature increase ( $\Delta\bar{T} = \Delta\bar{T}_{top} + \Delta\bar{T}_{middle} + \Delta\bar{T}_{bottom}$ ),  $I$  is solar intensity,  $A$  is area exposed to the solar energy source, and  $\Delta t$  is the exposure time.

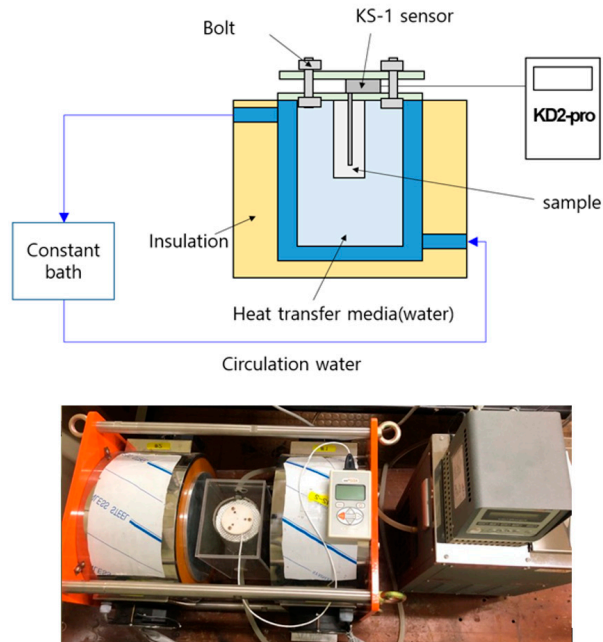


Figure 2. Schematic and photo of thermal conductivity experiment setup.

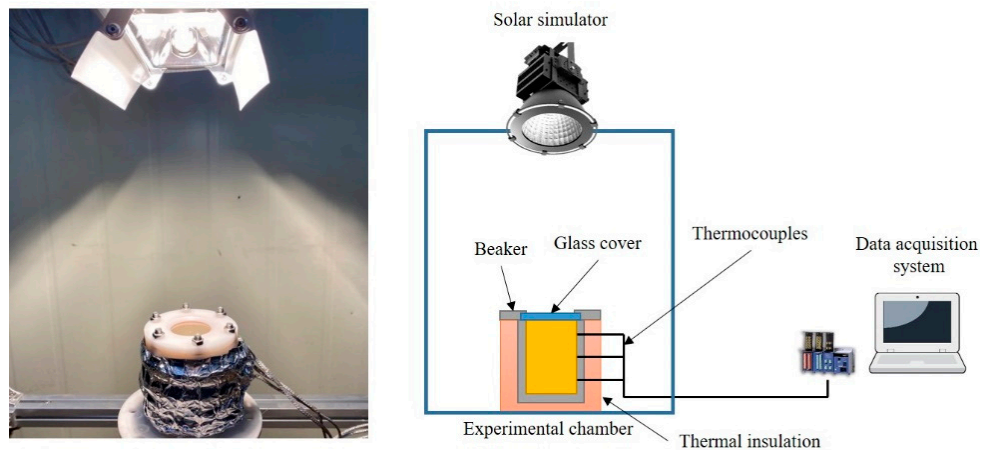


Figure 3. Schematic and picture of the photothermal energy conversion (PTEC) experiment setup.

The PTEC efficiency of  $Co_{0.5}Zn_{0.5}Fe_2O_4$  nanoparticles can also be defined using the specific absorption rate (SAR): the solar energy per unit mass absorbed by the nanoparticles, which can be calculated using Equation (4) [45]

$$SAR = \frac{m_{bf}c_{bf}}{1000m_p} \left( \frac{\Delta\bar{T}_{nf}}{\Delta t} - \frac{\Delta\bar{T}_{bf}}{\Delta t} \right) \tag{4}$$

where  $m_p$  and  $m_{bf}$  are nanoparticles and base fluid mass sample, respectively;  $c_{bf}$  is the base fluid specific heat;  $\Delta\bar{T}_{bf}$  and  $\Delta\bar{T}_{nf}$  are temperature elevation of the base fluid and nanofluid, respectively, at a given time  $\Delta t$ .

Table 2 presents the specification of measurement sensors used in this study. Thermal conductivity meter with an error of  $\pm 5\%$  was used to measure the thermal conductivity and viscometer with an error of 1% was used to measure the viscosity of nanofluid. Besides, the irradiance meter with an error of  $\pm 5\%$  was used to measure the irradiance of light. Moreover, the calculated error of measurements was too little, so that it was insignificant to present in this study.

**Table 2.** Specifications of experimental equipment.

Item	Thermal Conductivity Meter	Viscometer	Spectrometer	K-Type Thermocouple	Irradiance Meter
Measurement range	0.02–2 W/m $^{\circ}$ C	0.3–10,000 mPa·s	200–1300 nm	–200–1300 $^{\circ}$ C	0–1500 W/m $^2$
Accuracy	$\pm 5\%$	$\pm 1\%$	0.04–20 nm	$\pm 2.2$ $^{\circ}$ C	$\pm 5\%$

### 3. Results and Discussion

A DI water based  $\text{Co}_{0.5}\text{Zn}_{0.5}\text{Fe}_2\text{O}_4$  nanofluid was prepared via chemical coprecipitation in a two-step manufacturing technique. The following section describes the  $\text{Co}_{0.5}\text{Zn}_{0.5}\text{Fe}_2\text{O}_4$  nanoparticles characterization. Furthermore, magnetic, morphological, and thermophysical properties of the  $\text{Co}_{0.5}\text{Zn}_{0.5}\text{Fe}_2\text{O}_4$  nanofluid were experimentally investigated. The PTEC characteristics of the  $\text{Co}_{0.5}\text{Zn}_{0.5}\text{Fe}_2\text{O}_4$  nanofluid are discussed and compared to those of DI water.

#### 3.1. Characterization of $\text{Co}_{0.5}\text{Zn}_{0.5}\text{Fe}_2\text{O}_4$ Nanofluid

The synthesized  $\text{Co}_{0.5}\text{Zn}_{0.5}\text{Fe}_2\text{O}_4$  nanoparticles were examined via XRD, which is typically applied to examine the crystal structure of nanoparticles to identify crystalline forms in material. To perform the test, an X-ray was beamed at the particle and the scattering intensity in an outward direction was measured. Figure 4 presents an outline of the formation of  $\text{Co}_{0.5}\text{Zn}_{0.5}\text{Fe}_2\text{O}_4$  nanoparticles in this study. All the peak reflections in the XRD pattern were classified and refinement of the lattice parameter is denoted by (111), (200), (211), (300), (310), (311), and (332). The strongest reflection is observed from the (311) plane, indicating cubic spinel structure characteristics [46,47]. To calculate the average and maximum particle diameter of the  $\text{Co}_{0.5}\text{Zn}_{0.5}\text{Fe}_2\text{O}_4$  nanoparticles, Scherrer's equation [43] was applied, and the maximum and average diameters of the  $\text{Co}_{0.5}\text{Zn}_{0.5}\text{Fe}_2\text{O}_4$  nanoparticles were 18.07 nm and 14.73 nm, respectively.

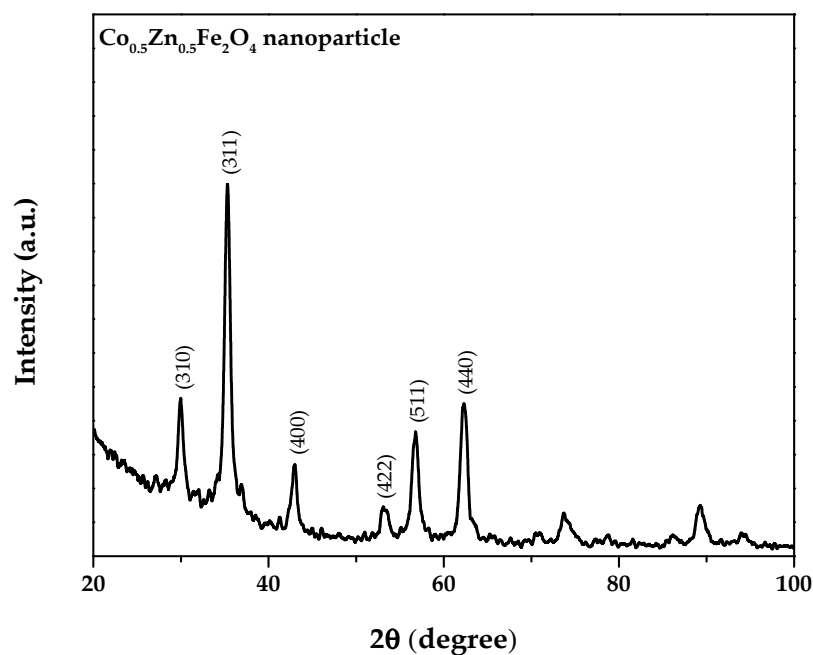


**Figure 4.** X-ray diffraction pattern of the  $\text{Co}_{0.5}\text{Zn}_{0.5}\text{Fe}_2\text{O}_4$  nanoparticle.

The  $\text{Co}_{0.5}\text{Zn}_{0.5}\text{Fe}_2\text{O}_4$  nanoparticle's morphology was examined via a high-resolution TEM test. The TEM imaging performed at two different scales (100 and 200 nm) is shown in Figure 5. The TEM image indicates that  $\text{Co}_{0.5}\text{Zn}_{0.5}\text{Fe}_2\text{O}_4$  nanoparticles are spherical shaped with diameters of 15–25 nm. The obtained results are well fit with XRD inspection result. Furthermore, it was observed that the  $\text{Co}_{0.5}\text{Zn}_{0.5}\text{Fe}_2\text{O}_4$  nanoparticles are uniformly distributed in the base fluid.

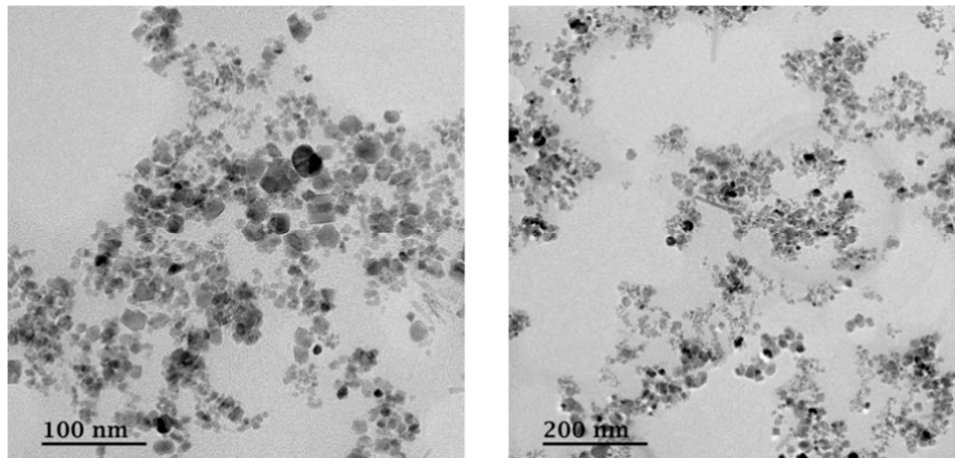


Figure 5. Transmission electron microscopy image of the  $\text{Co}_{0.5}\text{Zn}_{0.5}\text{Fe}_2\text{O}_4$  nanoparticles.

The ferrofluid's performance is directly affected by its magnetic characteristics. The VSM spectrum of the  $\text{Co}_{0.5}\text{Zn}_{0.5}\text{Fe}_2\text{O}_4$  nanoparticles is presented in Figure 6, with the VSM curve indicating that the  $\text{Co}_{0.5}\text{Zn}_{0.5}\text{Fe}_2\text{O}_4$  nanoparticles exhibit superparamagnetic behavior. Notably, ferrite nanoparticles exhibit superparamagnetic characteristics such that every nanoparticle may be regarded as thermally excited magnets in the sample. The maximum magnetization ( $M_s$ ) of  $\text{Co}_{0.5}\text{Zn}_{0.5}\text{Fe}_2\text{O}_4$  was 46.39 emu/g (electromagnetic units per gram).

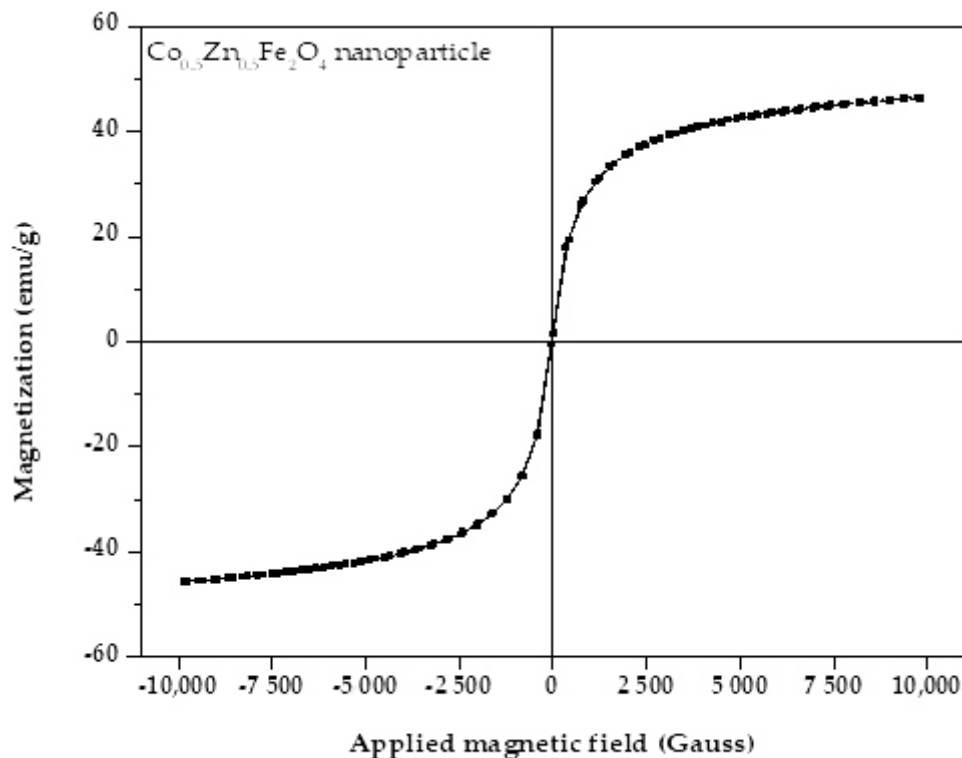


Figure 6. Vibrating sample magnetometry (VSM) spectrum of the  $\text{Co}_{0.5}\text{Zn}_{0.5}\text{Fe}_2\text{O}_4$  nanoparticles.

One of the primary concerns in nanofluid preparation is the prevention of nanoparticle agglomeration and settlement in the nanofluid. The nanofluid dispersion stability is a fundamental property that significantly influences the thermal and rheological characteristics of sample nanofluid. The absolute value of the zeta potential measurement is extensively used in various methods for examining nanofluid dispersion stability. Generally, an absolute zeta potential of  $>30$  mV is considered a reasonable absolute zeta potential value for obtaining a well-dispersed nanofluid. Figure 7 presents the  $\text{Co}_{0.5}\text{Zn}_{0.5}\text{Fe}_2\text{O}_4$  nanofluid zeta potential analysis. The average absolute zeta potential of the  $\text{Co}_{0.5}\text{Zn}_{0.5}\text{Fe}_2\text{O}_4$  nanofluid was  $-54.03$  mV, indicating high dispersion stability and that the  $\text{Co}_{0.5}\text{Zn}_{0.5}\text{Fe}_2\text{O}_4$  nanoparticles were well and uniformly dispersed in the DI water.

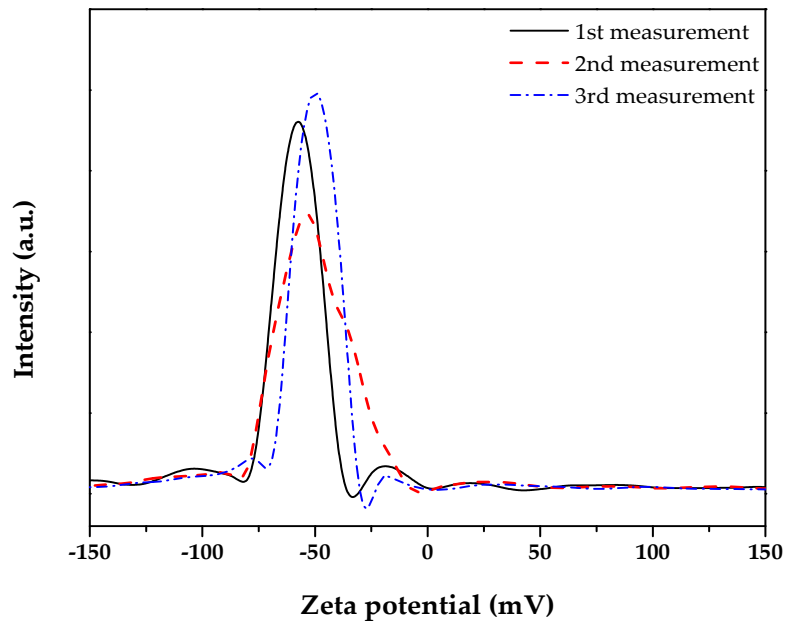


Figure 7. Zeta potential analysis of the  $\text{Co}_{0.5}\text{Zn}_{0.5}\text{Fe}_2\text{O}_4$  nanofluid.

Table 3 presents the relation between dispersion stability of the nanofluid and zeta potential value [48]. From Table 3, the  $\text{Co}_{0.5}\text{Zn}_{0.5}\text{Fe}_2\text{O}_4$  nanofluid can be considered as having great dispersion stability based on its absolute zeta potential.

Table 3. Absolute zeta potential values.

Zeta Potential (mV)	Stability
0–15	No stability
15–30	Moderate stability
30–45	High dispersion stability, low tendency to settle to the bottom
45–60	Great stability

Figure 8 illustrates the optical absorption behavior of the  $\text{Co}_{0.5}\text{Zn}_{0.5}\text{Fe}_2\text{O}_4$  nanofluid in the UV–Vis wavelength range of 300–1300 nm, and shows that all samples of the  $\text{Co}_{0.5}\text{Zn}_{0.5}\text{Fe}_2\text{O}_4$  nanofluid exhibit superior optical absorption in comparison with the base fluid. Furthermore, optical absorption spectra of the  $\text{Co}_{0.5}\text{Zn}_{0.5}\text{Fe}_2\text{O}_4$  nanofluid elevated with increasing nanofluid concentration. In all  $\text{Co}_{0.5}\text{Zn}_{0.5}\text{Fe}_2\text{O}_4$  nanofluid samples, the optical absorption decreased around a wavelength of 700–1200 nm, however the optical absorption of DI water increased in this range. It was observed that adding  $\text{Co}_{0.5}\text{Zn}_{0.5}\text{Fe}_2\text{O}_4$  nanoparticles to DI water changes the optical absorption characteristics of the DI water, improving absorption ability in the working fluid.

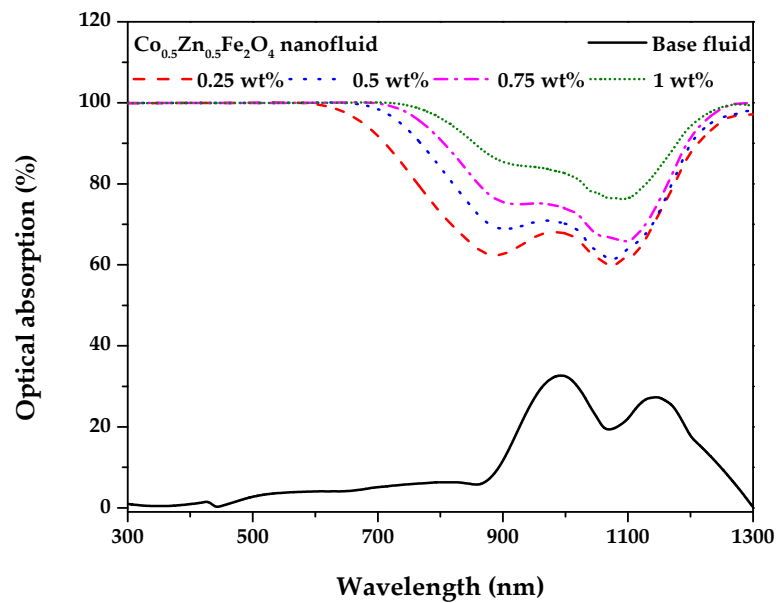


Figure 8. Optical absorption of the  $\text{Co}_{0.5}\text{Zn}_{0.5}\text{Fe}_2\text{O}_4$  nanofluid at different concentrations.

### 3.2. Viscosity and Thermal Conductivity of the $\text{Co}_{0.5}\text{Zn}_{0.5}\text{Fe}_2\text{O}_4$ Nanofluid

The viscosity of working fluid is one of the most important and fundamental properties, which can directly influence the thermal efficiency of system, operating cost, and applications area. Figure 9 presents the viscosity of the  $\text{Co}_{0.5}\text{Zn}_{0.5}\text{Fe}_2\text{O}_4$  nanofluid according to the nanofluid concentration at different temperatures. Moreover, the viscosity of the  $\text{Co}_{0.5}\text{Zn}_{0.5}\text{Fe}_2\text{O}_4$  nanofluid increased as the nanofluid concentration increased, in contrast, the viscosity decreased with increasing its temperature.

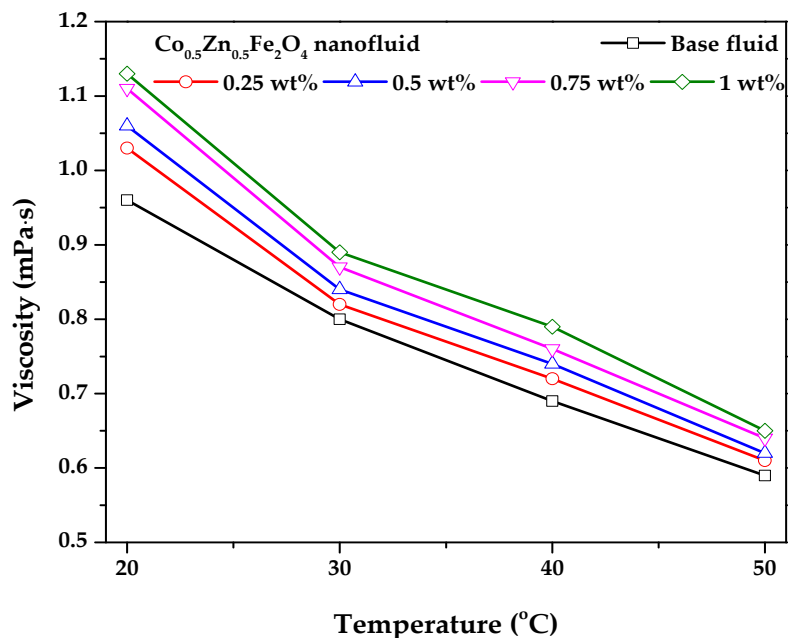


Figure 9. Viscosity of the  $\text{Co}_{0.5}\text{Zn}_{0.5}\text{Fe}_2\text{O}_4$  nanofluid at different concentrations.

For instance, the viscosities of 0.25 wt% and 1 wt%  $\text{Co}_{0.5}\text{Zn}_{0.5}\text{Fe}_2\text{O}_4$  nanofluid were 1.03 mPa·s and 1.13 mPa·s, respectively, which increased by 7.3% and 17.7%, respectively, in comparison with that of DI water at 20 °C. The measured viscosity of the water was 0.96 mPa·s and 0.59 mPa·s at 20 °C and 50 °C. It can be assumed that adding  $\text{Co}_{0.5}\text{Zn}_{0.5}\text{Fe}_2\text{O}_4$  nanoparticles to the DI water increases viscosity of the working fluid. Moreover, viscosities of 0.25 wt% and 1 wt%  $\text{Co}_{0.5}\text{Zn}_{0.5}\text{Fe}_2\text{O}_4$  nanofluid

decreased by 68.8% and 73.8% when the temperature decreased from 20 to 50 °C, which were 0.61 and 0.65 mPa·s, respectively. This could be explained by the enhanced collision between the nanoparticles in the  $\text{Co}_{0.5}\text{Zn}_{0.5}\text{Fe}_2\text{O}_4$  nanofluid [49]. The maximum viscosity of  $\text{Co}_{0.5}\text{Zn}_{0.5}\text{Fe}_2\text{O}_4$  nanofluid was 1.13 mPa·s at 1 wt% and 20 °C, respectively.

To investigate thermal conductivity and its enhancement of the  $\text{Co}_{0.5}\text{Zn}_{0.5}\text{Fe}_2\text{O}_4$  nanofluid, the conductivity of samples were measured according to temperature and concentration. The enhancement from thermal conductivity at the same temperature can be expressed by Equation (5).

$$k_{enh} = \left( \frac{k_{nf}}{k_{bf}} - 1 \right) \cdot 100 \quad (5)$$

where  $k_{bf}$  and  $k_{nf}$  are the thermal conductivity of the base fluid and  $\text{Co}_{0.5}\text{Zn}_{0.5}\text{Fe}_2\text{O}_4$  nanofluid, respectively.

The effects of temperature and concentration on the variation of thermal conductivity in the  $\text{Co}_{0.5}\text{Zn}_{0.5}\text{Fe}_2\text{O}_4$  nanofluid are presented in Figure 10. It has observed that the thermal conductivity improved when the concentration and operating time increased. The thermal conductivity of  $\text{Co}_{0.5}\text{Zn}_{0.5}\text{Fe}_2\text{O}_4$  nanofluid improved from 0.605 and 0.618 to 0.654 and 0.693 W/m·°C when the temperature increased from 20 to 50 °C at concentrations of 0.25 wt% and 1 wt%, respectively. The maximum thermal conductivity of  $\text{Co}_{0.5}\text{Zn}_{0.5}\text{Fe}_2\text{O}_4$  nanofluid reached up to 0.693 W/m·°C at a concentration and temperature of 1 wt% and 50 °C, respectively. It can be assumed that specific surface area expansion of  $\text{Co}_{0.5}\text{Zn}_{0.5}\text{Fe}_2\text{O}_4$  nanoparticles in nanofluid led to a higher heat transfer surface area and intense Brownian motion in the working fluid.

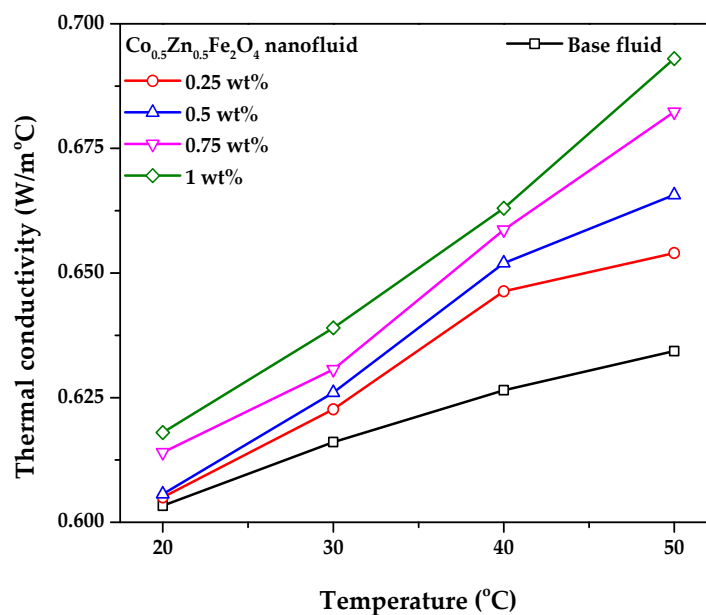


**Figure 10.** Thermal conductivity of the  $\text{Co}_{0.5}\text{Zn}_{0.5}\text{Fe}_2\text{O}_4$  nanofluid at different nanofluid concentrations.

Figure 11 illustrates the enhancement of thermal conductivity in the  $\text{Co}_{0.5}\text{Zn}_{0.5}\text{Fe}_2\text{O}_4$  nanofluid with various nanofluid concentrations at 20–50 °C. The enhancement of thermal conductivity in the  $\text{Co}_{0.5}\text{Zn}_{0.5}\text{Fe}_2\text{O}_4$  nanofluids were 3.1%, 4.9%, 7.5%, and 9.2% at concentrations of 0.25 wt%, 0.5 wt%, 0.75 wt%, and 1 wt%, respectively, at 50 °C. Brownian motion is the random collision between nanoparticles intensified under high concentration and temperature, hence improving the activation of nanofluid and heat transfer of the  $\text{Co}_{0.5}\text{Zn}_{0.5}\text{Fe}_2\text{O}_4$  nanofluid.

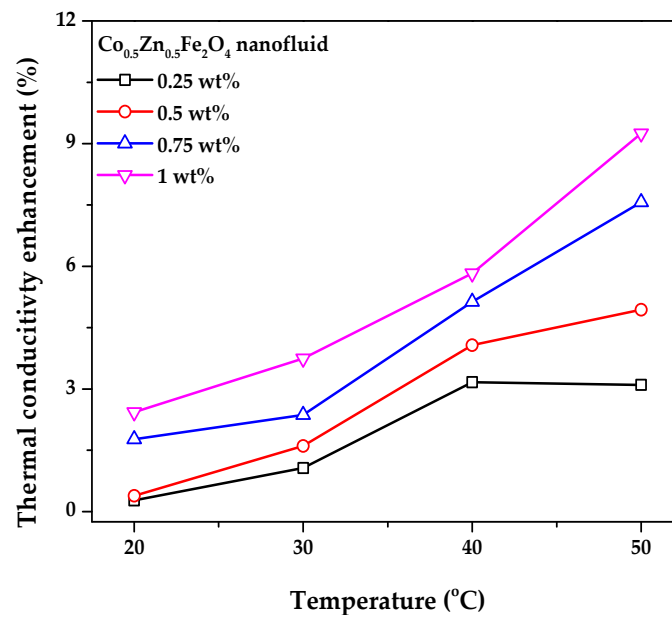


**Figure 11.** Thermal conductivity enhancement of the  $\text{Co}_{0.5}\text{Zn}_{0.5}\text{Fe}_2\text{O}_4$  nanofluid at different nanofluid concentrations.

### 3.3. PTEC Characterization of the $\text{Co}_{0.5}\text{Zn}_{0.5}\text{Fe}_2\text{O}_4$ Nanofluid

Figure 12 presents the variation of temperature in the DI water and the  $\text{Co}_{0.5}\text{Zn}_{0.5}\text{Fe}_2\text{O}_4$  nanofluid according to the exposure time for various concentrations. To examine the PTEC efficiency of the  $\text{Co}_{0.5}\text{Zn}_{0.5}\text{Fe}_2\text{O}_4$  nanofluid, the incident solar irradiance and ambient temperature were maintained at  $650 \text{ W/m}^2$  and  $20 \text{ }^\circ\text{C}$ , respectively. For all the samples, the temperature of the working fluid showed an increase tendency with operating time. The temperature increase in the  $\text{Co}_{0.5}\text{Zn}_{0.5}\text{Fe}_2\text{O}_4$  nanofluid was more remarkable at all  $\text{Co}_{0.5}\text{Zn}_{0.5}\text{Fe}_2\text{O}_4$  nanofluid concentrations, in comparison with DI water. The final temperature of the samples were  $46.4 \text{ }^\circ\text{C}$ ,  $49 \text{ }^\circ\text{C}$ ,  $49.6 \text{ }^\circ\text{C}$ ,  $50 \text{ }^\circ\text{C}$ , and  $48.7 \text{ }^\circ\text{C}$ , respectively, for DI water, and 0.25 wt%, 0.5 wt%, 0.75 wt%, and 1 wt%  $\text{Co}_{0.5}\text{Zn}_{0.5}\text{Fe}_2\text{O}_4$  nanofluid, after a solar exposure time of 120 min under. The maximum temperature increase for the  $\text{Co}_{0.5}\text{Zn}_{0.5}\text{Fe}_2\text{O}_4$  nanofluid was 7.7% more than that for the DI water, and it was obtained at 0.75 wt%. This enhanced PTEC performance is primarily caused by the superior thermal conductivity and optical absorption of the  $\text{Co}_{0.5}\text{Zn}_{0.5}\text{Fe}_2\text{O}_4$  nanofluid. Furthermore, temperature of the  $\text{Co}_{0.5}\text{Zn}_{0.5}\text{Fe}_2\text{O}_4$  nanofluid elevated as the concentration increased, except for 1 wt%  $\text{Co}_{0.5}\text{Zn}_{0.5}\text{Fe}_2\text{O}_4$  nanofluid. It can be inferred that this is primarily because the highly concentrated high-temperature nanoparticles in the 1 wt%  $\text{Co}_{0.5}\text{Zn}_{0.5}\text{Fe}_2\text{O}_4$  nanofluid agglomerated easily. Based on the PTEC test results for the  $\text{Co}_{0.5}\text{Zn}_{0.5}\text{Fe}_2\text{O}_4$  nanofluid in this study, 0.75 wt% was the optimal concentration for PTEC applications.

For a thorough investigation of the PTEC performance, three K-type temperature sensors were placed in the sample container. By measuring the temperature variation of the three thermocouples, which were installed in the vertical direction, the PTEC performance and temperature gradient of the bulk fluid under sunlight can be investigated. Figure 13 presents the temperature gradient of the DI water and  $\text{Co}_{0.5}\text{Zn}_{0.5}\text{Fe}_2\text{O}_4$  nanofluid with different concentrations. The temperature at the top of the bulk fluid was much higher than that at the middle and bottom due to the nanofluid solar weighted absorption fraction [22]. In this study, the temperature gaps between the top and bottom portions were  $14.5 \text{ }^\circ\text{C}$ ,  $17.6 \text{ }^\circ\text{C}$ ,  $18.2 \text{ }^\circ\text{C}$ ,  $18.8 \text{ }^\circ\text{C}$ , and  $18.6 \text{ }^\circ\text{C}$ , respectively, for DI water and 0.25 wt%, 0.5 wt%, 0.75 wt%, and 1 wt%  $\text{Co}_{0.5}\text{Zn}_{0.5}\text{Fe}_2\text{O}_4$  nanofluid. In addition, the temperature gap between the top and bottom position rose slightly with the concentration increase. The highest temperature gap was  $18.8 \text{ }^\circ\text{C}$ , which was observed in the 0.75 wt%  $\text{Co}_{0.5}\text{Zn}_{0.5}\text{Fe}_2\text{O}_4$  nanofluid. The nanofluid concentration with the highest temperature increased the performance of PTEC.

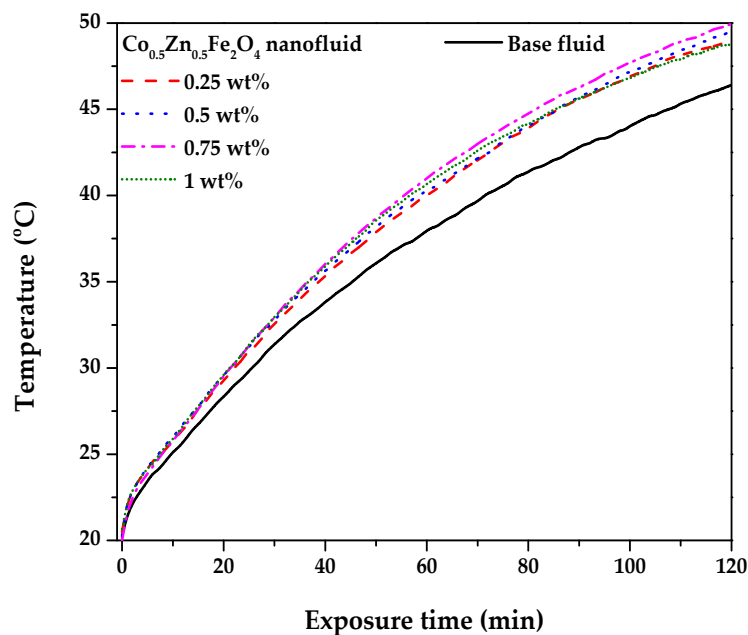


Figure 12. Temperature variation of base fluid and the  $\text{Co}_{0.5}\text{Zn}_{0.5}\text{Fe}_2\text{O}_4$  nanofluid.

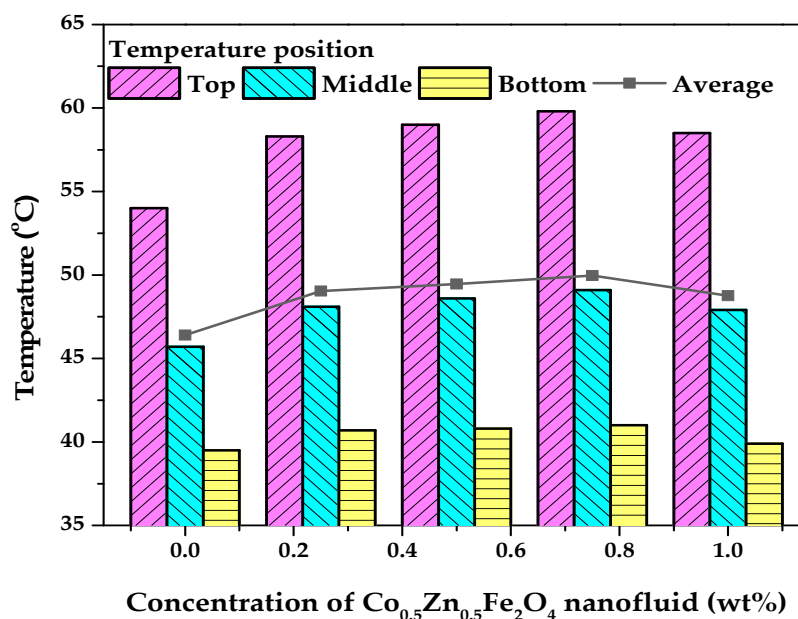
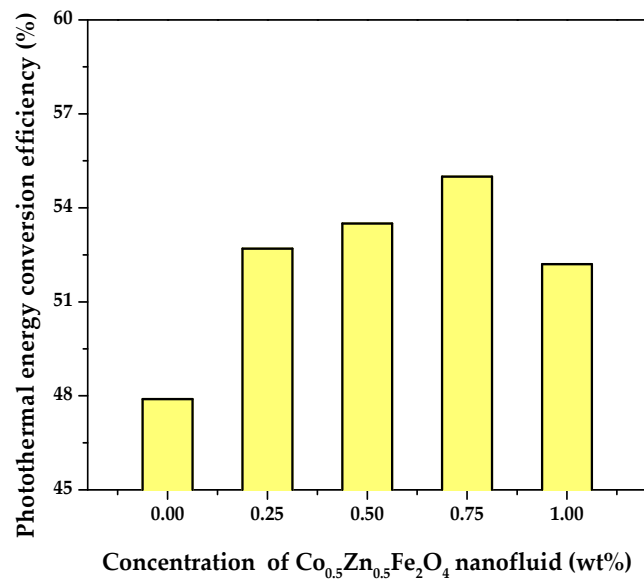


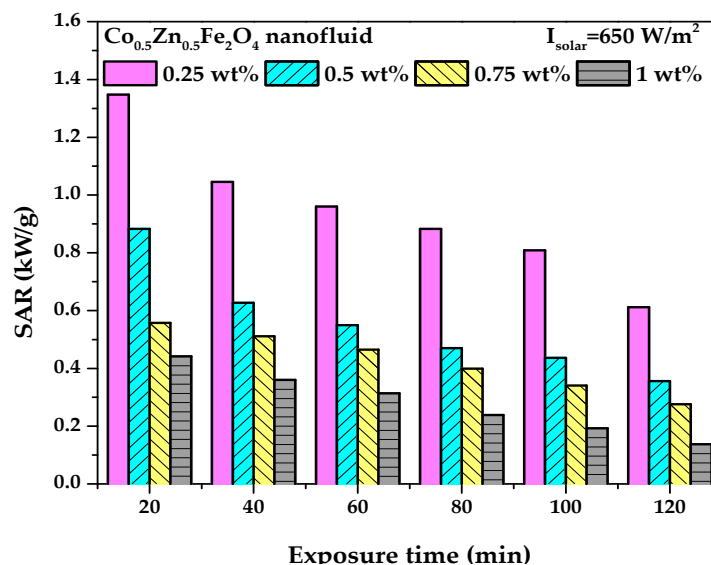
Figure 13. Temperature gradient of the  $\text{Co}_{0.5}\text{Zn}_{0.5}\text{Fe}_2\text{O}_4$  nanofluid as a function of concentration.

Figure 14 presents the PTEC efficiency of the DI water and the  $\text{Co}_{0.5}\text{Zn}_{0.5}\text{Fe}_2\text{O}_4$  nanofluid at different concentrations. The PTEC efficiency of the  $\text{Co}_{0.5}\text{Zn}_{0.5}\text{Fe}_2\text{O}_4$  nanofluid grows with an increase of concentration. After 120 min, the lowest PTEC efficiency was 47.9%, which was observed in the DI water. At the time, the PTEC efficiency of the  $\text{Co}_{0.5}\text{Zn}_{0.5}\text{Fe}_2\text{O}_4$  nanofluid was 52.7%, 53.5%, 55%, and 52.2% at concentrations of 0.25 wt%, 0.5 wt%, 0.75 wt%, and 1 wt%, respectively. The increase in PTEC efficiency of the  $\text{Co}_{0.5}\text{Zn}_{0.5}\text{Fe}_2\text{O}_4$  nanofluid was 4.8%, 5.6%, 7.1%, and 4.1% at concentrations of 0.25 wt%, 0.5 wt%, 0.75 wt%, and 1 wt%, respectively, in comparison with DI water. The highest PTEC efficiency of  $\text{Co}_{0.5}\text{Zn}_{0.5}\text{Fe}_2\text{O}_4$  nanofluid was 55%, and was observed at a concentration of 0.75 wt%. As shown in Figure 12, the temperature in the  $\text{Co}_{0.5}\text{Zn}_{0.5}\text{Fe}_2\text{O}_4$  nanofluid increased as the concentration increased, except for concentration of 1 wt%  $\text{Co}_{0.5}\text{Zn}_{0.5}\text{Fe}_2\text{O}_4$ ; and the similar trend was observed in the variation in the PTEC efficiency.



**Figure 14.** Photothermal conversion efficiency of the  $\text{Co}_{0.5}\text{Zn}_{0.5}\text{Fe}_2\text{O}_4$  nanofluid with various concentrations.

Figure 15 presents the variation in the SAR according to exposure time at different concentrations of the  $\text{Co}_{0.5}\text{Zn}_{0.5}\text{Fe}_2\text{O}_4$  nanofluid. The maximum SAR was achieved during the initial stage at 20 min, and the SAR decreased with exposure time for all concentrations. Furthermore, the SAR decreased rapidly with an increase in  $\text{Co}_{0.5}\text{Zn}_{0.5}\text{Fe}_2\text{O}_4$  nanofluid concentration, which is similar to the previous studies on the SAR of different nanofluids [44,45]. The highest SAR for the  $\text{Co}_{0.5}\text{Zn}_{0.5}\text{Fe}_2\text{O}_4$  nanofluid was 1.34 kW/g at a concentration of 0.25 wt% and an exposure time of 20 min. The SAR for the 0.25 wt% and 1 wt%  $\text{Co}_{0.5}\text{Zn}_{0.5}\text{Fe}_2\text{O}_4$  nanofluid decreased from 1.34 and 0.44 to 0.61 and 0.13 kW/g, respectively, under an incident solar irradiance of  $650 \text{ W/m}^2$ .



**Figure 15.** Variation in the specific absorption rate (SAR) of the  $\text{Co}_{0.5}\text{Zn}_{0.5}\text{Fe}_2\text{O}_4$  nanofluid at different concentrations.

#### 4. Conclusions

In this study,  $\text{Co}_{0.5}\text{Zn}_{0.5}\text{Fe}_2\text{O}_4$  nanoparticles were manufactured by using the chemical coprecipitation technique. The  $\text{Co}_{0.5}\text{Zn}_{0.5}\text{Fe}_2\text{O}_4$  nanoparticles were suspended in DI water (the base fluid) at different weight concentrations (0.25 wt%, 0.5 wt%, 0.75 wt%, and 1 wt%). TEM and XRD experiments were conducted to examine the nanostructure of the  $\text{Co}_{0.5}\text{Zn}_{0.5}\text{Fe}_2\text{O}_4$  nanoparticles.

Furthermore, the magnetic characteristics were examined using a VSM test at 25 °C. The thermal characteristics of the  $\text{Co}_{0.5}\text{Zn}_{0.5}\text{Fe}_2\text{O}_4$  nanofluid were investigated, including absolute zeta potential, optical absorption, viscosity, thermal conductivity, and PTEC. The following results were obtained:

- From the XRD results, the average and maximum diameter of the  $\text{Co}_{0.5}\text{Zn}_{0.5}\text{Fe}_2\text{O}_4$  particles were 14.73 nm and 18.7 nm, respectively. The saturation magnetization of the  $\text{Co}_{0.5}\text{Zn}_{0.5}\text{Fe}_2\text{O}_4$  nanoparticles was 46.57 emu/g, indicating that the  $\text{Co}_{0.5}\text{Zn}_{0.5}\text{Fe}_2\text{O}_4$  nanofluid could be classified as a magnetic nanofluid. The thermal conductivity of  $\text{Co}_{0.5}\text{Zn}_{0.5}\text{Fe}_2\text{O}_4$  nanofluid improved from 0.605 and 0.618 to 0.654 and 0.693 W/m·°C at concentrations of 0.25 wt% and 1 wt%, respectively, when the temperature increased from 20 to 50 °C. The maximum thermal conductivity of the  $\text{Co}_{0.5}\text{Zn}_{0.5}\text{Fe}_2\text{O}_4$  nanofluid reached up to 0.693 W/m·°C, which was obtained at 1 wt% and 50 °C. Adding  $\text{Co}_{0.5}\text{Zn}_{0.5}\text{Fe}_2\text{O}_4$  nanoparticles to DI water improved the optical absorption performance of the working fluid;
- The PTEC performance enhanced with the nanofluid concentration and exposure time. However, the highest temperature (50 °C) was observed in the 0.75 wt%  $\text{Co}_{0.5}\text{Zn}_{0.5}\text{Fe}_2\text{O}_4$  nanofluid. After 120 min, the PTEC efficiency of the  $\text{Co}_{0.5}\text{Zn}_{0.5}\text{Fe}_2\text{O}_4$  nanofluid was 52.7%, 53.5%, 55%, and 52.2% at concentrations of 0.25, 0.5, 0.75, and 1 wt%, respectively. The highest SAR of the  $\text{Co}_{0.5}\text{Zn}_{0.5}\text{Fe}_2\text{O}_4$  nanofluid was 1.34 kW/g at a concentration of 0.25 wt% and an exposure time of 20 min.

In the case of a magnetic nanofluid, it is important to develop a new alternative method to synthesize nanoparticles over previous complicated techniques that require expensive equipment. Moreover, it is necessary to study to replace the expensive and complex manufacturing nanoparticles and a method to secure high dispersion stability of the magnetic nanofluid in thermal systems. Presumably, the downside of the  $\text{Co}_{0.5}\text{Zn}_{0.5}\text{Fe}_2\text{O}_4$  nanofluid is a high viscosity, which can increase the pressure drop and pump power consumption in a heat transfer system. The magnetic field effect on thermal characteristics and PTEC performance of  $\text{Co}_{0.5}\text{Zn}_{0.5}\text{Fe}_2\text{O}_4$  nanofluid will be the focus of a forthcoming study.

**Author Contributions:** Conceptualization, H.C. and T.B.; methodology J.H.; validation, H.C., J.H.; formal analysis, T.B.; investigation, T.B.; resources, H.C.; writing—original draft preparation, T.B.; writing—review and editing, J.H. and H.C.; visualization, T.B.; supervision, H.C. All authors have read and agreed to the published version of the manuscript.

**Funding:** This study was supported by research fund from Chosun University, 2020.

**Conflicts of Interest:** The authors declare no conflict of interest.

## References

1. International Energy Agency. *World Energy Outlook 2019*; International Energy Agency: Paris, France, 2019.
2. Wen, D.; Lin, G.; Vafaei, S.; Zhang, K. Review of nanofluids for heat transfer applications. *Particuology* **2009**, *7*, 141–150. [[CrossRef](#)]
3. Sun, B.; Guo, Y.; Yang, D.; Li, H. The effect of constant magnetic field on convective heat transfer of  $\text{Fe}_3\text{O}_4$ /water magnetic nanofluid in horizontal circular tubes. *Appl. Therm. Eng.* **2020**, *171*, 114920. [[CrossRef](#)]
4. Esmaeili, E.; Ghazanfar, C.; Rounaghi, S.A. The influence of the alternating magnetic field on the convective heat transfer properties of  $\text{Fe}_3\text{O}_4$ -containing nanofluids through the Neel and Brownian mechanisms. *Appl. Therm. Eng.* **2017**, *110*, 1212–1219. [[CrossRef](#)]
5. Ghasemian, M.; Najafian, Z.; Goharkhah, M.; Ashjaee, M. Heat transfer characteristics of  $\text{Fe}_3\text{O}_4$  ferrofluid flowing in a mini channel under constant and alternating magnetic fields. *J. Magn. Magn. Mater.* **2015**, *381*, 158–167. [[CrossRef](#)]
6. Sheikholeslami, M.; Ganji, D. Nanofluid convective heat transfer using semi analytical and numerical approaches: A review. *J. Taiwan Inst. Chem. Eng.* **2016**, *65*, 43–77. [[CrossRef](#)]
7. Soltani, F.; Toghraie, D.; Karimipour, A. Experimental measurements of thermal conductivity of engine oil-based hybrid and mono nanofluids with tungsten oxide ( $\text{WO}_3$ ) and MWCNTs inclusions. *Powder Technol.* **2020**, *371*, 37–44. [[CrossRef](#)]

8. Sarbolookzadeh Harandi, S.; Karimipour, A.; Afrand, M.; Akbari, M.; D’Orazio, A. An experimental study on thermal conductivity of F-MWCNTs–Fe<sub>3</sub>O<sub>4</sub>/EG hybrid nanofluid: Effects of temperature and concentration. *Int. Commun. Heat Mass Transf.* **2016**, *76*, 171–177. [[CrossRef](#)]
9. Baghbanzadeh, M.; Rashidi, A.; Rashtchian, D.; Lotfi, R.; Amrollahi, A. Synthesis of spherical silica/multiwall carbon nanotubes hybrid nanostructures and investigation of thermal conductivity of related nanofluids. *Thermochim. Acta* **2012**, *549*, 87–94. [[CrossRef](#)]
10. Bahrami, M.; Akbari, M.; Karimipour, A.; Afrand, M. An experimental study on rheological behavior of hybrid nanofluids made of iron and copper oxide in a binary mixture of water and ethylene glycol: Non-Newtonian behavior. *Exp. Therm. Fluid Sci.* **2016**, *79*, 231–237. [[CrossRef](#)]
11. Afrand, M.; Toghraie, D.; Ruhani, B. Effects of temperature and nanoparticles concentration on rheological behavior of Fe<sub>3</sub>O<sub>4</sub>–Ag/EG hybrid nanofluid: An experimental study. *Exp. Therm. Fluid Sci.* **2016**, *77*, 38–44. [[CrossRef](#)]
12. Afrand, M. Experimental study on thermal conductivity of ethylene glycol containing hybrid nano-additives and development of a new correlation. *Appl. Therm. Eng.* **2017**, *110*, 1111–1119. [[CrossRef](#)]
13. Choi, S.U.S.; Eastman, J. Enhancing thermal conductivity of fluids with nanoparticles. In Proceedings of the 1995 International Mechanical Engineering Congress and Exhibition, San Francisco, CA, USA, 12–17 November 1995; p. 66.
14. Amjad, M.; Jin, H.; Du, X.; Wen, D. Experimental photothermal performance of nanofluids under concentrated solar flux. *Solar Energy Mater. Solar Cells* **2018**, *182*, 255–262. [[CrossRef](#)]
15. Chen, M.; He, Y.; Zhu, J.; Shuai, Y.; Jiang, B.; Huang, Y. An experimental investigation on sunlight absorption characteristics of silver nanofluids. *Solar Energy* **2015**, *115*, 85–94. [[CrossRef](#)]
16. Rativa, D.; Gómez-Malagón, L.A. Solar radiation absorption of nanofluids containing metallic nanoellipsoids. *Solar Energy* **2015**, *118*, 419–425. [[CrossRef](#)]
17. He, Q.; Wang, S.; Zeng, S.; Zheng, Z. Experimental investigation on photothermal properties of nanofluids for direct absorption solar thermal energy systems. *Energy Convers. Manag.* **2013**, *73*, 150–157. [[CrossRef](#)]
18. Qu, J.; Tian, M.; Han, X.; Zhang, R.; Wang, Q. Photo-thermal conversion characteristics of MWCNT–H<sub>2</sub>O nanofluids for direct solar thermal energy absorption applications. *Appl. Therm. Eng.* **2017**, *124*, 486–493. [[CrossRef](#)]
19. He, Y.; Chen, M.; Wang, X.; Hu, Y. Plasmonic multi-thorny Gold nanostructures for enhanced solar thermal conversion. *Solar Energy* **2018**, *171*, 73–82. [[CrossRef](#)]
20. Wang, X.; He, Y.; Hu, Y.; Jin, G.; Jiang, B.; Huang, Y. Photothermal-conversion-enhanced photocatalytic activity of flower-like CuS superparticles under solar light irradiation. *Solar Energy* **2018**, *170*, 586–593. [[CrossRef](#)]
21. Hazra, S.K.; Ghosh, S.; Nandi, T.K. Photo-thermal conversion characteristics of carbon black-ethylene glycol nanofluids for applications in direct absorption solar collectors. *Appl. Therm. Eng.* **2019**, *163*, 114402. [[CrossRef](#)]
22. Tong, Y.; Boldoo, T.; Ham, J.; Cho, H. Improvement of PTEC performance of MWCNT/Fe<sub>3</sub>O<sub>4</sub> hybrid nanofluid compared to Fe<sub>3</sub>O<sub>4</sub> nanofluid. *Energy* **2020**, *196*, 117086. [[CrossRef](#)]
23. Nkurikiyimfura, I.; Wang, Y.; Pan, Z. Heat transfer enhancement by magnetic nanofluids—A review. *Renew. Sustain. Energy Rev.* **2013**, *21*, 548–561. [[CrossRef](#)]
24. Novopashin, S.A.; Serebryakova, M.A.; Khmel, S.Y. Methods of magnetic fluid synthesis (review). *Thermophys. Aeromech.* **2015**, *22*, 397–412. [[CrossRef](#)]
25. Stephen Papell, S. Low Viscosity Magnetic Fluid Obtained by the Colloidal Suspension of Magnetic Particles. US Patent 3215572A, 2 November 1965.
26. López, J.; González-Bahamón, L.F.; Prado, J.; Caicedo, J.C.; Zambrano, G.; Gómez, M.E.; Esteve, J.; Prieto, P. Study of magnetic and structural properties of ferrofluids based on cobalt–zinc ferrite nanoparticles. *J. Magn. Magn. Mater.* **2012**, *324*, 394–402. [[CrossRef](#)]
27. Philip, J.; Damodaran, S.P.; Raj, B. Enhancement of thermal conductivity in magnetite based nanofluid due to chainlike structures. *Appl. Phys. Lett.* **2007**, *91*, 203108. [[CrossRef](#)]
28. Abareshi, M.; Goharshadi, E.; Zebarjad, S.; Khandan Fadafan, H.; Youssefi, A. Fabrication, Characterization and Measurement of Thermal Conductivity of Fe<sub>3</sub>O<sub>4</sub> Nanofluids. *J. Magn. Magn. Mater.* **2010**, *322*, 3895–3901. [[CrossRef](#)]
29. Djurek, I.; Znidarsic, A.; Kosak, A.; Djurek, D. Thermal conductivity measurements of the CoFe<sub>2</sub>O<sub>4</sub> and gamma-Fe<sub>2</sub>O<sub>3</sub> based nanoparticle ferrofluids. *Croat. Chem. Acta* **2007**, *80*, 529–532.

30. Aksenov, V.L.; Avdeev, M.V.; Balasoiu, M.; Bica, D.; Rosta, L.; Török, G.; Vekas, L. Aggregation in non-ionic water-based ferrofluids by small-angle neutron scattering. *J. Magn. Magn. Mater.* **2003**, *258–259*, 452–455. [[CrossRef](#)]
31. Karimi, A.; Afghahi, S.S.S.; Shariatmadar, H.; Ashjaee, M. Experimental investigation on thermal conductivity of  $MFe_2O_4$  ( $M=Fe$  and  $Co$ ) magnetic nanofluids under influence of magnetic field. *Thermochim. Acta* **2014**, *598*, 59–67. [[CrossRef](#)]
32. Sundar, L.; Singh, M.; Ramana, E.; Singh, B.; Grácio, J.; Sousa, A. Enhanced Thermal Conductivity and Viscosity of Nanodiamond-Nickel Nanocomposite Nanofluids. *Sci. Rep.* **2014**, *4*, 4039. [[CrossRef](#)]
33. Altan, C.; Elkatmış, A.; Aslan, N.; Bucak, S. Enhancement of thermal conductivity upon application of magnetic field to  $Fe_3O_4$  nanofluids. *J. Appl. Phys.* **2011**, *110*, 093917. [[CrossRef](#)]
34. Azizian, R.; Doroodchi, E.; Moghtaderi, B. Influence of Controlled Aggregation on Thermal Conductivity of Nanofluids. *J. Heat Transf.* **2015**, *138*. [[CrossRef](#)]
35. Parekh, K.; Lee, H. Experimental Investigation of Thermal Conductivity of magnetic nanofluids. *AIP Conf. Proc.* **2012**, *1447*, 385–386.
36. Arana, M.; Bercoff, P.G.; Jacobo, S.E. Thermomagnetic characterization of organic-based ferrofluids prepared with Ni ferrite nanoparticles. *Mater. Sci. Eng. B* **2017**, *215*, 1–8. [[CrossRef](#)]
37. Nabeel Rashin, M.; Hemalatha, J. Magnetic and ultrasonic studies on stable cobalt ferrite magnetic nanofluid. *Ultrasonics* **2014**, *54*, 834–840. [[CrossRef](#)] [[PubMed](#)]
38. Nabeel Rashin, M.; Hemalatha, J. Magnetic and ultrasonic investigations on magnetite nanofluids. *Ultrasonics* **2012**, *52*, 1024–1029. [[CrossRef](#)] [[PubMed](#)]
39. Chopkar, M.; Sudarshan, S.; Das, P.K.; Manna, I. Effect of Particle Size on Thermal Conductivity of Nanofluid. *Metall. Mater. Trans. A* **2008**, *39*, 1535–1542. [[CrossRef](#)]
40. Li, Q.; Xuan, Y.; Wang, J. Experimental investigations on transport properties of magnetic fluids. *Exp. Therm. Fluid Sci.* **2005**, *30*, 109–116. [[CrossRef](#)]
41. Hatami, N.; Kazemnejad Banari, A.; Malekzadeh, A.; Pouranfard, A.R. The effect of magnetic field on nanofluids heat transfer through a uniformly heated horizontal tube. *Phys. Lett. A* **2017**, *381*, 510–515. [[CrossRef](#)]
42. Zablotsky, D.; Mezulis, A.; Blums, E. Surface cooling based on the thermomagnetic convection: Numerical simulation and experiment. *Int. J. Heat Mass Transf.* **2009**, *52*, 5302–5308. [[CrossRef](#)]
43. Dorofeev, G.A.; Streletskii, A.N.; Povstugar, I.V.; Protasov, A.V.; Elsukov, E.P. Determination of nanoparticle sizes by X-ray diffraction. *Colloid J.* **2012**, *74*, 675–685. [[CrossRef](#)]
44. Jin, H.; Lin, G.; Bai, L.; Amjad, M.; Bandarra Filho, E.P.; Wen, D. Photothermal conversion efficiency of nanofluids: An experimental and numerical study. *Solar Energy* **2016**, *139*, 278–289. [[CrossRef](#)]
45. Bandarra Filho, E.P.; Mendoza, O.S.H.; Beicker, C.L.L.; Menezes, A.; Wen, D. Experimental investigation of a silver nanoparticle-based direct absorption solar thermal system. *Energy Conv. Manag.* **2014**, *84*, 261–267. [[CrossRef](#)]
46. Bragg, W.H. The Structure of Magnetite and the Spinels. *Nature* **1915**, *95*, 561. [[CrossRef](#)]
47. Vaidyanathan, G.; Sendhilnathan, S.; Arulmurugan, R. Structural and magnetic properties of  $Co_{1-x}Zn_xFe_2O_4$  nanoparticles by co-precipitation method. *J. Magn. Magn. Mater.* **2007**, *313*, 293–299. [[CrossRef](#)]
48. Kumar, A.; Dixit, C.K. 3—Methods for characterization of nanoparticles. In *Advances in Nanomedicine for the Delivery of Therapeutic Nucleic Acids*; Nimesh, S., Chandra, R., Gupta, N., Eds.; Woodhead Publishing: Cambridge, UK, 2017; pp. 43–58.
49. Malekzadeh, A.; Pouranfard, A.; Hatami, N.; Banari, A.; Rahimi, M.R. Experimental Investigations on the Viscosity of Magnetic Nanofluids under the Influence of Temperature, Volume Fractions of Nanoparticles and External Magnetic Field. *J. Appl. Fluid Mech.* **2016**, *9*, 693–697. [[CrossRef](#)]

**Publisher’s Note:** MDPI stays neutral with regard to jurisdictional claims in published maps and institutional affiliations.



© 2020 by the authors. Licensee MDPI, Basel, Switzerland. This article is an open access article distributed under the terms and conditions of the Creative Commons Attribution (CC BY) license (<http://creativecommons.org/licenses/by/4.0/>).